# Optical response with threefold symmetry axis on oriented microdomains of opal photonic crystals

L. C. Andreani, A. Balestreri, J. F. Galisteo-López,* M. Galli, and M. Patrini
*Department of Physics "A. Volta" and UdR CNISM, University of Pavia, Via Bassi 6, I-27100 Pavia, Italy*

E. Descrovi, A. Chiodoni, and F. Giorgis
*Materials and Microsystems Laboratory χ Lab, Physics Department, Polytechnic University of Torino, Corso Duca degli Abruzzi 24, I-10129 Torino, Italy*

L. Pallavidino and F. Geobaldo
*Materials Science and Chemical Engineering Department, Polytechnic University of Torino, Corso Duca degli Abruzzi 24, I-10129 Torino, Italy*

(Received 24 July 2008; revised manuscript received 9 October 2008; published 4 November 2008)

Opal photonic crystals viewed along the [111] direction of the fcc structure have a threefold symmetry axis; however this microscopic symmetry is difficult to observe in optical measurements performed on macroscopic areas containing microdomains with different orientations. In this work polarized transmittance measurements on [111]-stacked silica opals with single oriented microdomains, identified by field-emission scanning electron microscopy and laser-scanning confocal microscopy, demonstrate different optical response of twin structures with the two possible vertical stacking sequences. A detailed comparison with theory shows that microtransmittance experiments probe the photonic band structure along the Γ-*L*-*K* and Γ-*L*-*U* orientations of the Brillouin zone, respectively, thus giving conclusive evidence for macroscopic optical response related to the presence of a threefold (instead of a sixfold) symmetry axis in the photonic microstructure.

DOI: 10.1103/PhysRevB.78.205304 PACS number(s): 78.67.−n, 42.70.Qs, 42.25.Bs, 78.20.Bh

## I. INTRODUCTION

Opal-like structures, consisting of fcc lattices of dielectric spheres, are the most commonly studied example of a three-dimensional (3D) photonic crystal (PhC).[1–4] Artificial opals are produced by means of either sedimentation or vertical deposition on a glass substrate and are usually stacked along the [111] crystallographic direction of the fcc lattice.[5] Several studies of the optical properties of opals have been undertaken.[6–48] Much of the earlier research focused on the first-order stop band along the [111] direction (corresponding to a gap at the *L* point of the Brillouin zone) and on its evolution with the angle of incidence.[6–21,24,34] Polarization anisotropy effects have also been discussed.[9,23,28,40,42] Optical features at large angles arising from multiple Bragg coupling or diffraction have been investigated by several authors,[23,25,29,31,36] as well as optical spectra in the region of the second-order stop band with the important effects related to diffraction from high-energy bands.[32,33,35,45,46,48] Phase delay and group-velocity dispersion have also been determined.[7,19,38,46] Structural properties, especially in connection with stacking of lattice planes along the [111] direction and interplay of fcc versus other close-packed arrangements, have been thoroughly studied in recent years.[21,22,31,41,44,47]

It is well known that the [111] direction of the fcc structure is a rotation axis of order three (or threefold symmetry axis); however it is not easy to reveal the consequences of this microscopic property in optical spectra. The surface plane of a [111]-stacked opal[49] consists of a hexagonal lattice of spheres; hence an opal sample when observed with an optical microscope looks as having a sixfold symmetry. The presence of a threefold symmetry can only be recognized by looking at the plane of spheres just below the surface: there are two possible arrangements for this plane and they correspond to either the ABC,ABC,... or ACB,ACB,... stacking sequence in the close-packed fcc lattice.[50] Thus, verifying the effects of a threefold symmetry axis in the optical response is closely related to determining the stacking sequence in the microscopic structure.

Figure 1 shows a 3D view of the opal structure in direct space and of the Brillouin zone in reciprocal space. The *z* axis is taken along the [111] direction and the same choice of axes will be used throughout the paper. Panels a and b illustrate one of the two possible stacking sequences and the Brillouin zone in panel c corresponds to the same choice of orientation. The presence of a threefold symmetry axis is clearly seen from the figure. The correspondence between the orientations in direct and reciprocal spaces is most easily recognized by noting that the quadrant defining the Γ-*L*-*U* orientation in the Brillouin zone cuts the right square facet containing the *X* point and it corresponds to the right square facet in the 3D views of Figs. 1(a) and 1(b). On the other hand, the quadrant defining the Γ-*L*-*K* orientation cuts the left hexagonal facet containing another *L* point and it corresponds to the left hexagonal facet of Figs. 1(a) and 1(b).

Also, notice that the six Γ-*L*-*W* orientations in the upper face of the Brillouin zone are equivalent among themselves; in particular two opposite *LW* directions can be transformed into each other by reflection symmetry with respect to a Γ-*L*-*U* (or Γ-*L*-*K*) mirror plane. On the other hand, the three Γ-*L*-*K* orientations are equivalent among themselves but different from the Γ-*L*-*U* orientations: indeed, the two sets of orientations *cannot* be transformed into each other as the

 

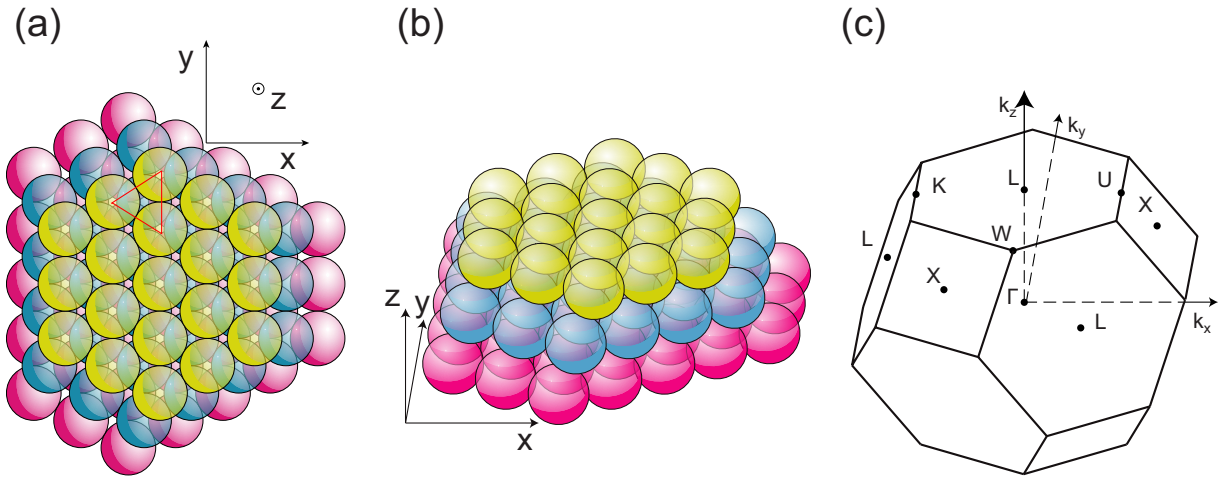


FIG. 1. (Color online) [(a) and (b)] Opal structure in direct space: (a) top and (b) side views. The $z$ axis is taken along the [111] direction. (c) fcc Brillouin zone with symmetry points. The triangle in (a) is placed with its center above one of the spheres of the second layer.

Γ-*L*-*W* plane is *not* a mirror plane of the fcc structure. These considerations are obviously in agreement with the group-theoretical analysis of eigenstates in opal-based photonic crystals.[51]

On the experimental side, optical properties at small values of the incidence angle are nearly isotropic and it is only at large angles that different orientations in a (111) plane can be distinguished. As we have just remarked, the six Γ-*L*-*W* orientations are equivalent among each other. Thus, verifying the presence of a threefold symmetry axis amounts to distinguishing between Γ-*L*-*K* and Γ-*L*-*U* orientations. However, opal samples as commonly grown are characterized by the presence of microdomains with twin structures, namely that of Fig. 1 and the one obtained by applying mirror reflection in the *yz* plane: thus any optical measurement performed on large areas yields an average over different domains and shows properties associated with sixfold rotation symmetry around the [111] direction. Furthermore, in a reflection experiment the optical beam crosses the sample in two opposite directions: again, the resulting reflection spectra are equivalent to averaging over two stacking sequences and display sixfold rotation symmetry.[52] It is only by performing transmission experiments at large angles on single-domain crystals that the presence of threefold rotation symmetry can become manifest in optical properties. While the presence of twin fcc structures in macrodomains and their effect on the optical properties have been studied by several authors,[17,40,42,44] oriented domains of a truly fcc lattice with well-defined stacking sequence were only observed by x-ray diffraction at grazing incidence[13] or in optical diffraction from colloidal structures.[22]

In this work we study artificial opals made of silica nanospheres that are shown to possess long strips corresponding to the two different stacking sequences of the fcc lattice. By field-emission scanning electron microscopy and by confocal microscopy, we are able to identify microdomains that correspond to a well-defined stacking sequence. Polarized transmission experiments up to large angles of incidence on such oriented microdomains give evidence of a different optical response that is related to the physically nonequivalent Γ-*L*-*K* and Γ-*L*-*U* orientations. A detailed comparison with theoretically calculated photonic bands and polarized spectra allows us to confirm the interpretation and to relate transmittance spectra with photonic bands for the respective orientations. The results give conclusive evidence for optical properties related to the presence of a threefold symmetry axis in the opal microstructure and, therefore, for the exact correspondence between symmetry properties at microscopic and macroscopic levels in these 3D photonic crystals.

## II. SAMPLES AND MICROSCOPIC CHARACTERIZATION

Silica nanospheres (430 nm diameter, 3%–4% polydispersity) were synthesized by a sol-gel procedure based on the Stöber-Fink-Bohn method, consisting of the hydrolysis and condensation of tetraethyl orthosilicate (TEOS) catalyzed by ammonia.[53,54] Artificial opals were successively grown by vertical deposition technique.[55,56] Such a self assembling method involves placing a nearly vertical glass substrate in aqueous suspension of nanospheres (0.5 vol %) previously obtained. The solvent evaporation performed under suitable conditions (temperature of 55 °C, atmospheric pressure) led to the deposition of ordered three-dimensional packing along the [111] crystallographic direction of the fcc lattice, having several square centimeter dimensions parallel to the glass substrate and a thickness varying between 4 and 15 layers of spheres. The sample regions chosen for optical characterization, several $mm^2$ in extension, had 12 layers as determined from an analysis of the optical response.[38]

Initial morphological characterization was performed employing optical microscopy. The experimental geometry, as well as the collected images, are shown in Fig. 2. When illuminated under normal incidence as in Fig. 2(a), the samples are homogeneously colored, and present small domains in the form of strips which run parallel to the growth direction $y$ and are separated by macroscopic cracks [see Fig. 2(c)]. The strip width is in the 50–300 $\mu$m range. However, when the sample is illuminated at a finite angle as shown in Fig. 2(b), one can see that alternating domains, named 1 and 2, present different colors [see Fig. 2(d)]. Furthermore,

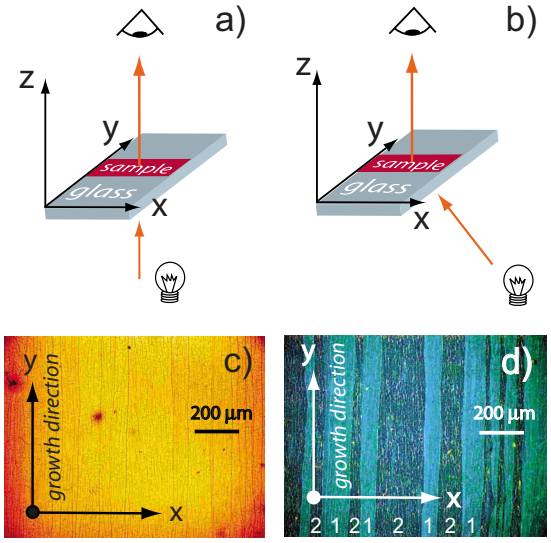


FIG. 2. (Color online) Observation of ordered domains under the optical microscope in transmitted light. [(a) and (b)] Illumination geometry with incident light at normal and oblique incidences, respectively. (c) With illumination at normal incidence, the sample appears homogeneous. (d) With illumination at oblique incidence, bright (type 1) and dark (type 2) regions become manifest. The $y$ axis in (c) and (d) is parallel to the direction of growth in the vertical deposition.

changing the sign of the angle of illumination reverses the colors observed in the two different types of domains.

The geometry of optical transmission experiments at oblique incidence is shown in Fig. 3(a) and light is focused onto the single domains or strips seen under the optical microscope. Thus, in order to characterize the structural properties of the single domains, we observed the sample surface under a field-emission scanning electron microscope (FESEM) (Zeiss Supra 40). Figure 3 shows FESEM images of sample regions corresponding to domains of types 1 and 2 [Figs. 3(b) and 3(d), respectively]. A large enough magnification was employed in order to appreciate the plane of spheres lying below the top surface. In these images, a chromatic bandpass filtering has been applied in order to emphasize the absence of nanospheres in the second fcc layer under particular interstices of the first layer [blue spots in Figs. 3(b) and 3(d)]. It can be seen that, in the two domains, the layer just below the surface takes one of the two possible positions when stacking hexagonal planes in a close packing arrangement, as indicated by the red triangles. Assuming that both domain types have fcc symmetry, the above observation indicates that each domain type possesses one of the two available stacking sequences for this particular crystal structure, namely ABCABC... or ACBACB…. Such peculiar pattern, with crystal domains parallel to the growth direction $y$ but oriented in different manner, is believed to have originated from convection fluxes of the colloidal suspension which have been shown to affect sample morphology.[31,57]

The different stacking sequences corresponding to the two domains are even better evidenced by laser scanning confocal microscopy (LSCM) (WITEC AlphaSNOM). In such a setup, the sample is raster scanned through the focal region of a high numerical aperture (NA) (=0.95) microscope objective. In Fig. 4 we show reflectance maps of two different layers for the two domains starting from the first layer [Figs. 4(a) and 4(c)] and moving to the second layer [Figs. 4(b) and 4(d)] of the artificial opal.[58] In Figs. 4(a) and 4(b), the circles are referred to the spheres of the first layer within domain 1

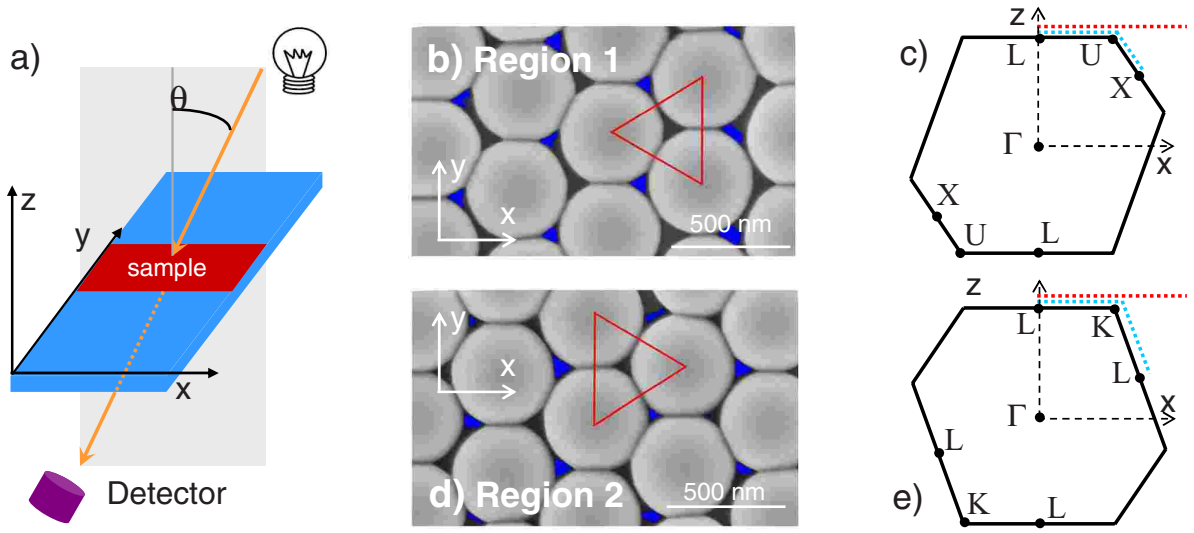


FIG. 3. (Color online) (a) Geometry of transmission experiments: light is incident from the top and has negative $k_x$ and $k_z$ components. (b) FESEM image of type-1 microdomain with (c) vertical cross section of Brillouin zone corresponding to the experimental geometry (only the relevant symmetry points are shown): the incident-beam probes the $\Gamma$-$L$-$U$ orientation. (d) FESEM image of type-2 microdomain with (e) vertical cross section of Brillouin zone corresponding to the experimental geometry: the incident-beam probes the $\Gamma$-$L$-$K$ orientation. The dotted lines in (c) and (e) indicate two paths in $k$ space, to be referred to later. The blue spots in (b) and (d), arising from a chromatic bandpass filtering, denote the absence of nanospheres in the second fcc layer below particular interstices of the first layer. The red triangles are placed with their center above one of the spheres of the second layer. Notice that type-1 domains in (b) have the same orientation as the schematic structure in Figs. 1(a) and 1(b).

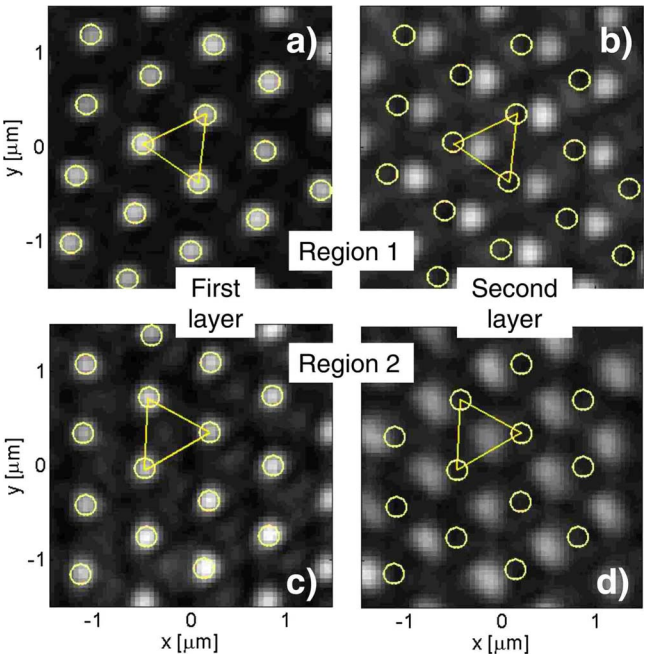


FIG. 4. (Color online) Confocal microscopy images of type-1 domains [top panels (a) and (b)] and of type-2 domains [bottom panels (c) and (d)]. Left panels [(a) and (c)] show reflectance maps of the first layers while right panels [(b) and (d)] show reflectance maps of the second layers. Yellow circles denote the sphere positions of the first layer.

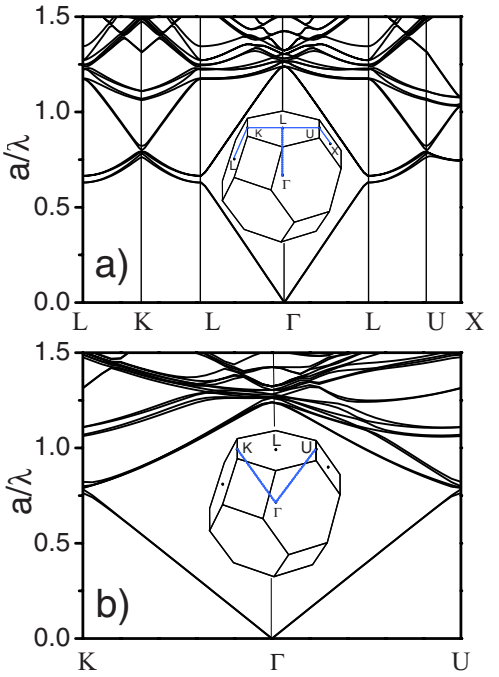


FIG. 5. (Color online) Calculated photonic bands of the infinite fcc lattice with close-packed silica spheres (dielectric constant $\epsilon = 2.1$) along two paths (a) on the surface and (b) inside the Brillouin zone, as indicated by the blue lines in the insets.

while the triangles emphasize the particular packing sequence in agreement with FESEM characterization. In Figs. 4(c) and 4(d) the other stacking sequence corresponding to domain 2 is shown. Altogether, structural information from FESEM and confocal microscopy yields clear-cut evidence of the presence of oriented domains with the two stacking sequences allowed for [111]-stacked fcc structure.

These structural observations allow us to align the sample prior to performing an optical characterization. Figures 3(c) and 3(e) show vertical cross sections of the Brillouin zone in the *xz* plane, relevant for transmission measurements for domains of types 1 and 2, respectively. The correspondence is most easily seen by noticing that domains of type 1 correspond to the orientation of the structure in Figs. 1(a) and 1(b) and indeed the cross section in Fig. 3(c) is oriented like the Brillouin zone in Fig. 1(c). In the present experimental geometry with the incident wave-vector components pointing along the negative *x* and *z* axes [see Fig. 3(a)] when probing a domain of type 1, the incident wave vector will probe the photonic band structure along a Γ-*L*-*U* orientation.[59] Notice that $\mathbf{k}=(k_x,k_z)$ with negative $k_x,k_z$ is equivalent to $-\mathbf{k}=(-k_x,-k_z)$: the relevant symmetry points are shown in the cross section of Fig. 3(c). On the other hand, if we consider a type 2 domain, the incident-beam probes the photonic bands along the Γ-*L*-*K* orientation and, again, Fig. 3(e) displays the relevant symmetry points. This should allow us to measure and distinguish the bands along the two orientations by just moving from one sample domain to another, with the experimental geometry kept fixed.

## III. OPTICAL MEASUREMENTS AND COMPARISON WITH THEORY

According to the above discussion we are now able to probe the optical properties along the Γ-*L*-*U* or Γ-*L*-*K* orientations, always under the assumption that our samples present an fcc crystal structure.[60] As mentioned before, we expect a different behavior for each case. This is evidenced in Fig. 5 by the photonic bands for the infinite ideal fcc lattice calculated by plane-wave expansion.[61,62] In Fig. 5(a) we show the usual representation of energy bands along a path connecting high-symmetry points on the surface of the fcc Brillouin zone. Here we can see how energy bands calculated along *L*-*K* and *L*-*U* directions in the upper hexagonal facet of the Brillouin zone are identical. It is only when the considered path moves away from the hexagonal facet that, along the *LK* and *UX* directions, the bands become different since no gap opens at the *X* point of the Brillouin zone.

The distinction between Γ-*L*-*U* and Γ-*L*-*K* orientations becomes more pronounced when taking into account energy bands inside the Brillouin zone. Figure 5(b) shows photonic bands calculated along the Γ*K* and Γ*U* directions. Here it is evident that although at the zone edge photonic modes in both directions have the same energy, for wave vectors inside the Brillouin zone the bands present quite a different behavior, which will determine a different optical response for the two orientations. Nevertheless the measurements at a fixed value of the incidence angle do not correspond to a straight line inside the Brillouin zone in wave-vector space but rather to a more complex curvilinear path that is not easy to visualize.

We now turn to the experimental results. Due to the microstructure of the samples, consisting of small domains pos-

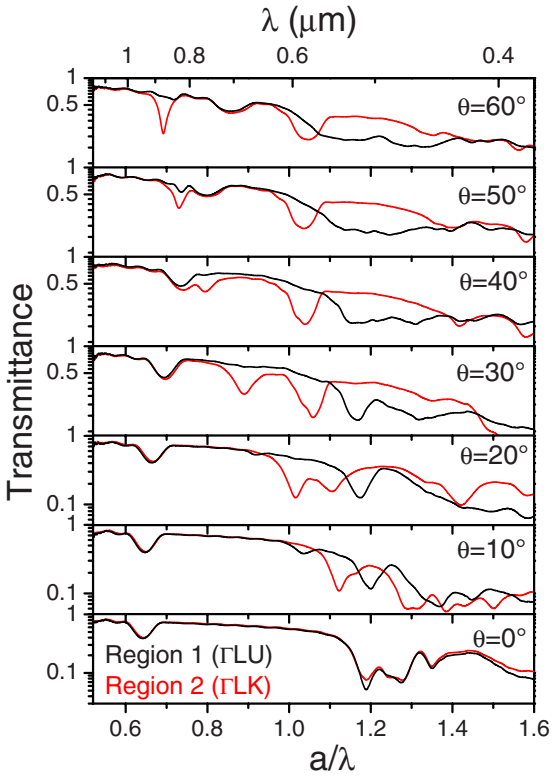


FIG. 6. (Color online) Unpolarized transmittance spectra for different angles of incidence on regions 1 (black line, Γ-*L*-*U* orientation) and 2 (red line, Γ-*L*-*K* orientation).

sessing different orientation, small probe beams were employed to avoid averaging the optical response of different domains. Transmission measurements have been performed by a microreflectometer setup[36,63] with a probe white light beam from a halogen lamp having a spot diameter of 100 $\mu$m and an angular aperture of 1°. Measurements were collected at increasing values of the angle of incidence in steps of 5°, either for unpolarized light or for both *s* and *p* input polarizations.

The difference between the Γ-*L*-*U* and Γ-*L*-*K* orientations can already be appreciated measuring the transmission for unpolarized light for domains of types 1 and 2, respectively. Results are shown in Fig. 6 for angles of incidence going from quasinormal incidence to 60°. It is evident from the measured spectra that the optical response is different if we increase the incidence angle along the Γ-*L*-*U* or Γ-*L*-*K* orientations. These differences become more pronounced in the high-energy region ($a/\lambda > 1$), where multiple Bragg diffraction by several families of crystallographic planes takes place[32,33,35,45,46,48] and the effects of a threefold symmetry axis on the optical properties are enhanced by Bragg scattering processes.

In order to better appreciate the differences between the optical response along the Γ-*L*-*U* and Γ-*L*-*K* orientations, we performed microtransmission measurements for *s*- and *p*-polarized input light, and represented the results in a contour plot. Figure 7 shows these results together with calculated bands. Photonic bands are plotted as a function of the incidence angle $\theta_{in}$ by relating the wave vector to the angle with $|(\mathbf{k}+\mathbf{G})_{\|}| = (\omega/c)\sin\theta_{in}$, where $\mathbf{G}$ is a reciprocal-lattice vector. Two sets of bands are shown: for wave vectors on the plane containing the upper facet of the fcc Brillouin zone (red lines), and along the surface of the Brillouin zone following the *LUX* and *LKL* paths (blue lines). For the latter case, only the first two bands are represented for the sake of clarity. The paths in *k* space for "red" and "blue" bands are those shown in Figs. 3(c) and 3(e), with the same convention of colors. As mentioned above, neither representation is rigorous; as in a transmission experiment we probe the eigenmodes inside the Brillouin zone and not only on its surface. Hence, an exact account for the optical response of the samples would come in principle from considering the energy bands inside the Brillouin zone together with the coupling efficiencies of the eigenmodes.[51] Nevertheless, we will see that, with the combination of the two sets of bands in Fig. 7, we can gather relevant information regarding the optical response of the sample.

Dark streaks in the contour plots of Fig. 7, corresponding to transmission dips in the measured spectra, closely match the dispersion of calculated bands even in the high-energy region. For lower energies a streak appears at $a/\lambda = 0.64$ for normal incidence and shifts to higher energies with increasing angle of incidence, corresponding to the *L* pseudogap associated with Bragg diffraction by the (111) planes parallel to the sample surface. For $\theta_{in} = 45°$ an anticrossing takes place between this structure and another one presenting a dispersion of opposite sign. It is at this point that clear differences between the Γ-*L*-*U* and Γ-*L*-*K* orientations become apparent. Besides the fact that the anticrossing is much more evident for the case of *p* polarization, as previously reported,[23] it can be seen that for the Γ-*L*-*K* orientation such anticrossing is more pronounced. This happens because the peak with negative dispersion is much more intense for the Γ-*L*-*K* orientation than for the Γ-*L*-*U* case. To understand this, one has to consider that the peak with negative dispersion, causing the anticrossing, comes from Bragg diffraction from adjacent families of planes such as (200) which are only excited for large incidence angles. When we increase the angle along the Γ-*L*-*U* orientation, the streak becomes barely noticeable, as a consequence of the absence of a Bragg peak along the Γ*X* direction for artificial opals.[64–66] On the other hand, on increasing the angle along the Γ-*L*-*K* orientation, we encounter a marked streak coming from Bragg diffraction by {111} families of planes not parallel to the surface such as the $(\bar{1}11)$ one.

In order to understand this behavior, we consider now the bands calculated along the surface of the Brillouin zone along the *LKL* and *LUX* paths [blue lines in Fig. 7, see also Fig. 5(a)]. These bands contain the information about Bragg diffraction processes by other families of planes different from the (111) ones parallel to the $\theta_{in}$ sample surface. If we consider energy bands for the Γ-*L*-*U* orientation along the *U*-*X* direction, we see that no gap is present and this corresponds to the absence of a noticeable streak in transmittance spectra for $\theta_{in} > 45°$. This coincides with the fact that no Bragg diffraction peak by (200) planes can be observed for the particular case of artificial opals along the Γ*X* direction in reciprocal space. On the other hand, along the Γ-*L*-*K* orientation there is a small but noticeable energy gap (which is

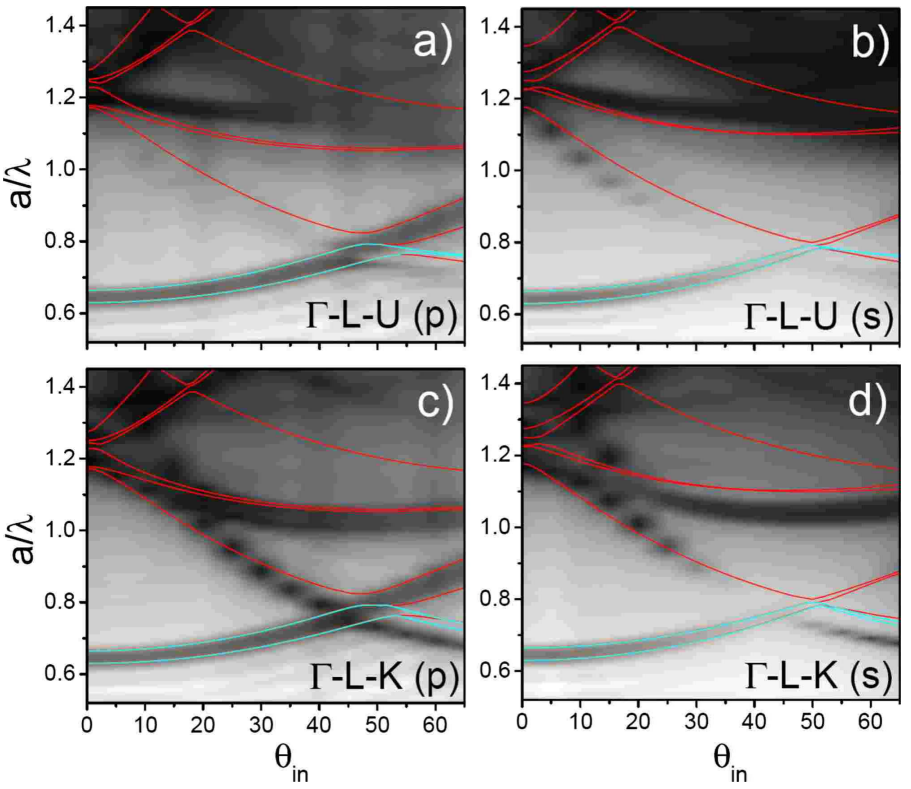


FIG. 7. (Color online) Contour plots of measured transmittance for *s*- or *p*-input polarization along the Γ-*L*-*U* or Γ-*L*-*K* orientations, as indicated. Superimposed red and blue lines correspond to calculated photonic bands along the paths shown in Figs. 3(c) and 3(e) (see text).

larger for *p* polarization) that corresponds to the visible streak in transmittance.

In Fig. 8 we show a contour plot of theoretically calculated transmission spectra. Calculations were performed with the scattering-matrix method described in Ref. 67. Calculated bands on a plane containing the upper facet of the Brillouin zone (red lines) and along the *LUX* and *LKL* paths (blue lines) are also shown, like in Fig. 7. A few comments can then be made. First, theoretical transmission spectra are in good overall agreement with the experimental ones (apart from generally lower experimental transmittance at high energies due to diffuse scattering). The same features noticed above on the anisotropy of the optical properties between Γ-*L*-*U* and Γ-*L*-*K* can be recognized. The agreement between experiment and theory is an additional proof for the observation of optical properties related to two twin structures in our samples, which are characteristic of the [111]-stacked fcc lattice. Finally, it is worth mentioning that rather thin samples (12 layers in the present case) can already reproduce the behavior predicted for the photonic bands of the infinite system.

The issue of possible presence of stacking faults is worth discussing. In principle, the observations by optical and confocal microscopies as well as FESEM cannot distinguish between the absence of stacking faults and their appearance in pairs. However, the occurrence of random pairs of opposite stacking faults would largely eliminate the difference in optical response between two domains since the transmitted beam in any domain would probe both Γ-*L*-*U* and Γ-*L*-*K* orientations. Thus, our observations of a large difference in the optical response together with the general agreement between experiment and theory point against this possibility. Also, we notice that in thin-film samples produced by dip coating the convective fluxes along the growth direction (studied, e.g., in Ref. 31), together with the low growth rate, play an important role in reducing the concentration of stacking faults and in improving the sample homogeneity. Indeed, both our microscopic and optical observations point to a very good homogeneity of the samples within each domain. Of course, a possible small concentration of stacking faults cannot be excluded: this may be responsible for some of the residual discrepancies that appear in the comparison between Figs. 7 and 8. The possible occurrence and optical characterization of stacking faults *within each oriented domain* is a very interesting topic that is worth further investigations in the future.

## IV. CONCLUSIONS

We have performed structural and optical characterizations of thin artificial opals grown by vertical deposition with the goal of demonstrating the nonequivalence of Γ-*L*-*U* and Γ-*L*-*K* orientations in the optical properties. Such anisotropy, which can be observed in transmission (not in reflection) configuration, follows from the presence of a threefold symmetry axis in the microscopic fcc structure. The key observation, made with the optical microscope by illuminating at oblique incidence with respect to the [111] normal direction, is that the sample presents a series of narrow strips oriented along the growth direction which correspond to microscopic

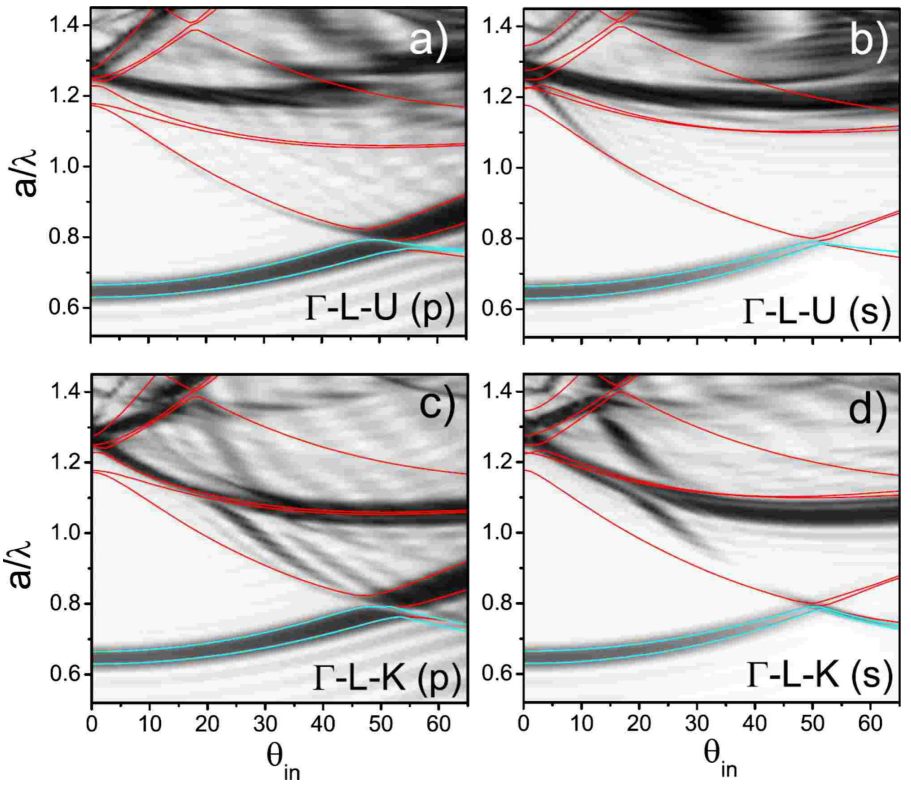


FIG. 8. (Color online) Contour plots of calculated transmittance for *s*- or *p*-input polarization along the Γ-*L*-*U* or Γ-*L*-*K* orientations, as indicated. Superimposed red and blue lines correspond to calculated photonic bands along the paths shown in Figs. 3(c) and 3(e) (see text).

domains of the two possible stacking sequences of the fcc structure. This observation is corroborated by field-emission scanning electron microscopy and by laser-scanning confocal microscopy, which allow visualization of the nanosphere layer below the surface and therefore assignment of the proper stacking sequence to each oriented microdomain.

These morphological and structural characterizations allow us to orient the samples prior to optical transmittance measurements, which are performed with a spot dimension of the order of the domain size to probe each single oriented domain. For a specified experimental geometry, the Γ-*L*-*U* and Γ-*L*-*K* orientations can be probed by moving from one microdomain to the other. Both unpolarized and polarized transmission spectra show clear evidence of nonequivalent optical properties along the Γ-*L*-*U* and Γ-*L*-*K* orientations. A detailed comparison with calculated photonic bands and transmittance allows us to interpret many physical features of the spectra and to associate the anisotropy to the effect of Bragg scattering from families of lattice planes other than the (111) one. Altogether, the experimental results show clear-cut evidence for the inequivalence of Γ-*L*-*U* and Γ-*L*-*K* orientations. The presence of a threefold symmetry axis has a marked effect on the optical transmittance at large angles when measured on properly oriented microdomains, thereby reconciling the symmetry of physical properties at microscopic and macroscopic levels.

## ACKNOWLEDGMENTS

Juan Galisteo-López was supported by the Postdoctoral Program of the Spanish Ministry of Science and Education. This work was supported by European Network of Excellence IST-2-511616-NOE (PHOREMOST), by the Project "Nanostructures for Applied Photonics" financed by Piedmont Region and by the CARIPLO Foundation.

*Present address: Instituto de Ciencia de Materiales de Madrid (CSIC), c/Sor Juana Inés de la Cruz 3, Madrid 28049, Spain

[1] E. Yablonovitch, Phys. Rev. Lett. **58**, 2059 (1987).
[2] S. John, Phys. Rev. Lett. **58**, 2486 (1987).
[3] J. D. Joannopoulos, S. G. Johnson, R. D. Meade, and J. N. Winn, *Photonic Crystals—Molding the Flow of Light*, 2nd ed. (Princeton University Press, Princeton, NJ, 2008).
[4] K. Sakoda, *Optical Properties of Photonic Crystals* (Springer-Verlag, New York, 2001).
[5] For a review, see, e.g. C. López, Adv. Mater. (Weinheim, Ger.) **15**, 1679 (2003).
[6] V. N. Astratov, V. N. Bogomolov, A. A. Kaplyanskii, A. V. Prokofiev, L. A. Samoilovich, S. M. Samoilovich, and Y. A. Vlasov, Nuovo Cimento Soc. Ital. Fis., D **17**, 1349 (1995).

[7] I. I. Tarhan, M. P. Zinkin, and G. H. Watson, Opt. Lett. **20**, 1571 (1995).
[8] W. L. Vos, R. Sprik, A. van Blaaderen, A. Imhof, A. Lagendijk, and G. H. Wegdam, Phys. Rev. B **53**, 16231 (1996).
[9] I. I. Tarhan and G. H. Watson, Phys. Rev. Lett. **76**, 315 (1996).
[10] V. N. Bogomolov, S. V. Gaponenko, I. N. Germanenko, A. M. Kapitonov, E. P. Petrov, N. V. Gaponenko, A. V. Prokofiev, A. N. Ponyavina, N. I. Silvanovich, and S. M. Samoilovich, Phys. Rev. E **55**, 7619 (1997).
[11] Yu. A. Vlasov, V. N. Astratov, O. Z. Karimov, A. A. Kaplyanskii, V. N. Bogomolov, and A. V. Prokofiev, Phys. Rev. B **55**, R13357 (1997).
[12] H. Míguez, C. López, F. Meseguer, A. Blanco, L. Vázquez, R. Mayoral, M. Ocaña, V. Fornés, and A. Mifsud, Appl. Phys. Lett. **71**, 1148 (1997).
[13] W. L. Vos, M. Megens, C. van Kats, and P. Bösecke, Langmuir **13**, 6004 (1997).
[14] J. E. G. J. Wijnhoven and W. L. Vos, Science **281**, 802 (1998).
[15] A. A. Zakhidov, R. H. Baughman, Z. Iqbal, C. Cui, I. Khayrullin, S. O. Dantas, J. I. Marti, and V. G. Ralchenko, Science **282**, 897 (1998).
[16] H. Míguez, A. Blanco, F. Meseguer, C. López, H. M. Yates, M. E. Pemble, V. Fornés, and A. Mifsud, Phys. Rev. B **59**, 1563 (1999).
[17] Y. A. Vlasov, S. Petit, G. Klein, B. Honerlage, and C. Hirlimann, Phys. Rev. E **60**, 1030 (1999).
[18] M. S. Thijssen, R. Sprik, J. E. G. J. Wijnhoven, M. Megens, T. Narayanan, A. Lagendijk, and W. L. Vos, Phys. Rev. Lett. **83**, 2730 (1999).
[19] A. Imhof, W. L. Vos, R. Sprik, and A. Lagendijk, Phys. Rev. Lett. **83**, 2942 (1999).
[20] A. Blanco, E. Chomski, S. Grabtchak, M. Ibisate, S. John, S. W. Leonard, C. López, F. Meseguer, H. Miguez, J. P. Mondia, G. A. Ozin, O. Toader, and H. M. van Driel, Nature (London) **405**, 437 (2000).
[21] Yu. A. Vlasov, V. N. Astratov, A. V. Baryshev, A. A. Kaplyanskii, O. Z. Karimov, and M. F. Limonov, Phys. Rev. E **61**, 5784 (2000).
[22] R. M. Amos, J. G. Rarity, P. R. Tapster, T. J. Shepherd, and S. C. Kitson, Phys. Rev. E **61**, 2929 (2000).
[23] H. M. van Driel and W. L. Vos, Phys. Rev. B **62**, 9872 (2000).
[24] Yu. A. Vlasov, X. Z. Bo, J. C. Sturm, and D. J. Norris, Nature (London) **414**, 289 (2001).
[25] S. G. Romanov, T. Maka, C. M. Sotomayor Torres, M. Müller, R. Zentel, D. Cassagne, J. Manzanares-Martinez, and C. Jouanin, Phys. Rev. E **63**, 056603 (2001).
[26] J. F. Galisteo López and W. L. Vos, Phys. Rev. E **66**, 036616 (2002).
[27] V. N. Astratov, A. M. Adawi, S. Fricker, M. S. Skolnick, D. M. Whittaker, and P. N. Pusey, Phys. Rev. B **66**, 165215 (2002).
[28] J. F. Galisteo-López, F. López-Tejeira, S. Rubio, C. López, and J. Sánchez-Dehesa, Appl. Phys. Lett. **82**, 4068 (2003).
[29] J. F. Galisteo-López, E. Palacios-Lidón, E. Castillo-Martínez, and C. López, Phys. Rev. B **68**, 115109 (2003).
[30] L. M. Goldenberg, J. Wagner, J. Stumpe, B.-R. Paulke, and E. Görnitz, Physica E (Amsterdam) **17**, 433 (2003).
[31] K. Wostyn, Y. Zhao, B. Yee, K. Clays, A. Persoons, G. de Schaetzen, and L. Hellemans, J. Chem. Phys. **118**, 10752 (2003).
[32] J. F. Galisteo-López and C. López, Phys. Rev. B **70**, 035108 (2004).
[33] H. Míguez, V. Kitaev, and G. A. Ozin, Appl. Phys. Lett. **84**, 1239 (2004).
[34] A. V. Baryshev, A. A. Kaplyanskii, V. A. Kosobukin, K. B. Samusev, D. E. Usvyat, and M. F. Limonov, Phys. Rev. B **70**, 113104 (2004).
[35] F. Garcia-Santamaria, J. F. Galisteo-López, P. V. Braun, and C. López, Phys. Rev. B **71**, 195112 (2005).
[36] E. Pavarini, L. C. Andreani, C. Soci, M. Galli, F. Marabelli, and D. Comoretto, Phys. Rev. B **72**, 045102 (2005).
[37] G. von Freymann, S. John, S. Wong, V. Kitaev, and G. A. Ozin, Appl. Phys. Lett. **86**, 053108 (2005).
[38] J. F. Galisteo-López, M. Galli, M. Patrini, A. Balestreri, L. C. Andreani, and C. López, Phys. Rev. B **73**, 125103 (2006).
[39] S. Gottardo, M. Burresi, F. Geobaldo, L. Pallavidino, F. Giorgis, and D. S. Wiersma, Phys. Rev. E **74**, 040702(R) (2006).
[40] A. V. Baryshev, A. B. Khanikaev, H. Uchida, M. Inoue, and M. F. Limonov, Phys. Rev. B **73**, 033103 (2006).
[41] A. V. Baryshev, V. A. Kosobukin, K. B. Samusev, D. V. Usvyat, and M. F. Limonov, Phys. Rev. B **73**, 205118 (2006).
[42] A. V. Baryshev, A. B. Khanikaev, R. Fujikawa, H. Uchida, and M. Inoue, Phys. Rev. B **76**, 014305 (2007).
[43] M. Ishii, M. Harada, A. Tsukigase, and H. Nakamura, J. Opt. A, Pure Appl. Opt. **9**, S372 (2007).
[44] X. Checoury, S. Enoch, C. López, and A. Blanco, Appl. Phys. Lett. **90**, 161131 (2007).
[45] L. A. Dorado, R. A. Depine, G. Lozano, and H. Miguez, Phys. Rev. B **76**, 245103 (2007).
[46] J. F. Galisteo-López, M. Galli, A. Balestreri, M. Patrini, L. C. Andreani, and C. López, Opt. Express **15**, 15342 (2007).
[47] E. Vekris, V. Kitaev, D. D. Perovic, J. S. Aitchison, and G. A. Ozin, Adv. Mater. (Weinheim, Ger.) **20**, 1110 (2008).
[48] S. G. Romanov, M. Bardosova, I. M. Povey, M. E. Pemble, and C. M. Sotomayor Torres, Appl. Phys. Lett. **92**, 191106 (2008).
[49] We avoid speaking of a [111] orientation, as most commonly done in the literature, since we reserve this expression for the nonequivalent Γ-*L*-*U* and Γ-*L*-*K* orientations that are the focus of this work.
[50] N. W. Ashcroft and N. D. Mermin, *Solid State Physics* (Holt-Saunders, Philadelphia, 1976).
[51] F. López-Tejeira, T. Ochiai, K. Sakoda, and J. Sánchez-Dehesa, Phys. Rev. B **65**, 195110 (2002).
[52] We have verified this statement by numerical calculation of reflectance spectra on finite-size opals with different orientations using the Fourier-modal or scattering-matrix method described in Ref. 67.
[53] W. Stöber, A. Fink, and E. Bohn, J. Colloid Interface Sci. **26**, 62 (1968).
[54] D. A. Santamaria Razo, L. Pallavidino, E. Garrone, F. Geobaldo, E. Descrovi, A. Chiodoni, and F. Giorgis, J. Nanopart. Res. **10**, 1225 (2008).
[55] P. Jiang, J. F. Bertone, K. S. Hwang, and V. L. Colvin, Chem. Mater. **11**, 2132 (1999).
[56] L. Pallavidino, D. Santamaria Razo, F. Geobaldo, A. Balestreri, D. Bajoni, M. Galli, L. C. Andreani, C. Ricciardi, E. Celasco, M. Quaglio, and F. Giorgis, J. Non-Cryst. Solids **352**, 1425 (2006).
[57] D. J. Norris, E. G. Arlinghaus, L. Meng, R. Heiny, and L. E. Scriven, Adv. Mater. (Weinheim, Ger.) **16**, 1393 (2004).
[58] Notice that, using confocal microscopy in reflection mode, the images of the second layer are slightly distorted due to scattering

from interfaces in the first layer. As Fig. 4 shows, such a distortion does not impede the collection of optical images of the first two layers with reasonable quality. In Ref. 54 a characterization technique based on the confocal microscope is demonstrating that imaging of the first three layers of the opal is actually possible. As an alternative, fluorescence confocal microscopy using light emitting spheres could be used: see, e.g., V. Kitaev, S. Fournier-Bidoz, S. M. Yang, and G. A. Ozin, J. Mater. Chem. **12**, 966 (2002). Even in this case, however, distortion of the excitation laser spot, impinging on the second layer through the first one, cannot in principle be avoided.

[59] Notice that it is crucial to specify the experimental geometry: for example, if the beam would be incident from the top (negative $k_z$) but with a positive $k_x$ component, measurements on domain 1 would probe the $\Gamma$-*L*-*K* orientation, i.e., the roles of the two nonequivalent orientations would be reversed.

[60] This is verified by the anisotropy of the optical properties shown below. Also, we have direct evident of the fcc structure from confocal microscopy measurements with a deeper focus (not shown here, see Ref. 54).

[61] K. M. Ho, C. T. Chan, and C. M. Soukoulis, Phys. Rev. Lett. **65**, 3152 (1990).

[62] K. Busch and S. John, Phys. Rev. E **58**, 3896 (1998).

[63] M. Galli, M. Belotti, D. Bajoni, M. Patrini, G. Guizzetti, D. Gerace, M. Agio, L. C. Andreani, and Y. Chen, Phys. Rev. B **70**, 081307(R) (2004).

[64] E. Yablonovitch and T. J. Gmitter, Phys. Rev. Lett. **63**, 1950 (1989).

[65] A. Mihi, M. Ocana, and H. Miguez, Adv. Mater. (Weinheim, Ger.) **18**, 2244 (2006).

[66] J. F. Galisteo-López, M. Galli, A. Balestreri, L. C. Andreani, and C. López, Appl. Phys. Lett. **90**, 231112 (2007).

[67] A. Balestreri, L. C. Andreani, and M. Agio, Phys. Rev. E **74**, 036603 (2006).